Eur Biophys J (2007) 36:133–144
DOI 10.1007/s00249-006-0114-2

ARTICLE

Computational study of coagulation factor VIIa's affinity for phospholipid membranes

Olivier Taboureau · Ole Hvilsted Olsen

Received: 9 March 2006 / Revised: 12 September 2006 / Accepted: 31 October 2006 / Published online: 28 November 2006

Abstract The interaction between the γ-carboxyglutamic acid-rich domain of coagulation factor VIIa (FVIIa), a vitamin-K-dependent enzyme, and phospholipid membranes plays a major role in initiation of blood coagulation. However, despite a high sequence and structural similarity to the Gla domain of other vitamin-K-dependent enzymes with a high membrane affinity, its affinity for negatively charged phospholipids is poor. A few amino acid differences are responsible for this observation. Based on the X-ray structure of lysophosphatidylserine (lysoPS) bound to the Gla domain of bovine prothrombin (Prth), models of the Gla domain of wildtype FVIIa and mutated FVIIa Gla domains in complex with lysoPS were built. Molecular dynamics (MD) and steered molecular dynamics (SMD) simulations on the complexes were applied to investigate the significant difference in the binding affinity. The MD simulation approach provides a structural and dynamic support to the role of P10Q and K32E mutations in the improvement of the membrane contact. Hence, rotation of the Gly11 main chain generated during the MD simulation results in a hydrogen bond with Q10 side chain as well as the appearance of a hydrogen bond between E32 and Q10 forcing the loop harbouring Arg9 and Arg15 to shrink and thereby enhances the accessibility of the phospholipids to the calcium ions. Furthermore, the application of the SMD simulation method to dissociate C6-lysoPS from a series of Gla domain models exhibits a ranking of the rupture force that can be useful in the interpretation of the PS interaction with Gla domains. Finally, adiabatic mapping of Gla6 residue in FVIIa with or without insertion of Tyr4 confirms the critical role of the insertion on the conformation of the side chain Gla6 in FVIIa and the corresponding Gla7 in Prth.

Keywords Coagulation factor FVIIa · Gla domain · Lysophosphatidylserine · Membrane binding · Steered molecular dynamics · Molecular dynamics

Abbreviations

Gla	γ-carboxyglutamic acid
LysoPS	Lysophosphatidylserine
C6-lysoPS	Dicaproyphosphatidylserine
MD	Molecular dynamics
SMD	Steered molecular dynamics
Prth	Prothrombin
TF	Tissue factor
K_d	Dissociation constant
FVIIa	Coagulation factor VIIa

Introduction

Coagulation factor VIIa (FVIIa), a member of the family of vitamin-K-dependent plasma enzymes, is a central component in the initiation of blood coagulation. A complex formation with tissue factor (TF) is required to render FVIIa biologically active and activate blood-clotting factors IX and X (Davie et al. 1991; Furie and Furie 1992). To favour FVIIa/TF complex formation, interaction of FVIIa with negatively charged phospholipid membranes plays an important role (Furie and Furie 1988). This interaction

O. Taboureau · O. H. Olsen (✉)
Haemostasis Biochemistry, Novo Nordisk A/S, Novo Nordisk Park, Building G8.2.90, 2760 Måløv, Denmark
e-mail: oho@novonordisk.com

is probably mediated through a common mechanism of vitamin-K-dependent proteins involving the γ-carboxyglutamic acid domain (Gla) (Nelsestuen 1999).

The Gla domains consist of ~45 amino acid residues of which 9–12 glutamic acid residues are modified to Gla residues during post-translational carboxylation (Magnusson et al. 1974; Nelsestuen et al. 1974; Stenflo 1974). The Gla residues bind calcium ions, inducing a significant structural perturbation from a largely unfolded domain to the folded membrane-binding conformer (Grant et al. 2004). Despite a high degree of sequence and structural similarity of the different Gla domains, this family of proteins displays a broad range of affinities for negatively charged phospholipids. For example, the dissociation constants (K_d) for the bovine prothrombin (Prth) was determined to be ~150× lower than that of FVIIa despite a sequence homology of ~70% (McDonald et al. 1997). This variation in membrane binding ability was suggested to be mostly related to a few specific positions, namely positions 11, 33, 34 (Prth numbering) (Shen et al 1997, 1998). Mutants P10Q and Tyr4 insertion in FVIIa shows a 2-fold enhancement in membrane affinity while another double mutant P10Q/K32E shows a 25-fold enhancement in membrane affinity (Shah et al. 1998). The mutant with highest affinity, (Y4)P10Q/K32E/D33F/A34E) shows 150- to 300-fold improvement over wild type FVIIa. These membrane affinity enhancements were related to a similar improvement in their activity as coagulants. Indeed, the functional activity of these proteins was improved up till 40-fold depending on the assay method (Nelsestuen et al. 2001). Except for the insertion of Tyr4 in FVIIa, most of the mutations are in the region close to residue 32. This region is situated on the opposite side of the Gla domain relative to the common solvent-exposed hydrophobic patch (Phe4, Leu5 and Leu8 in FVIIa) and quite far from the N-terminal end of the protein, where the membrane contact is generally assumed (Freedman et al. 1996). This hydrophobic cluster belongs to an ~12 N-terminal residues loop identified as an ω-loop, based on its conformation, hydrophobic character and solvent exposure (Fetrow 1995). Based on several investigations, the ω-loop was suggested to contribute to the phospholipids membrane binding (Soriano-Garcia et al 1992; Zhang and Castellino 1994; Christiansen et al. 1995; Falls et al. 2001).

Recently, X-ray crystallographic structures of bovine Prth fragment 1 (Prth) and heteronuclear NMR spectroscopy studies of a selectively 15N-labelled peptide based on the sequence of the human Prth Gla domain, Prth (1–46), in complex with calcium and lysophosphatidylserine (lysoPS) allowed to identify critical interactions of lysoPS with Prth Gla domain (Huang et al. 2003). The serine head group binds calcium ions, Gla17 and Gla21. The glycerophosphate main chain binds to a positively charged patch formed by Lys3, Arg10 and Arg16. van der Waal (vdW) contacts between Phe5, Leu6 and Gla7 and the glycerol main chain were also observed (Fig. 1).

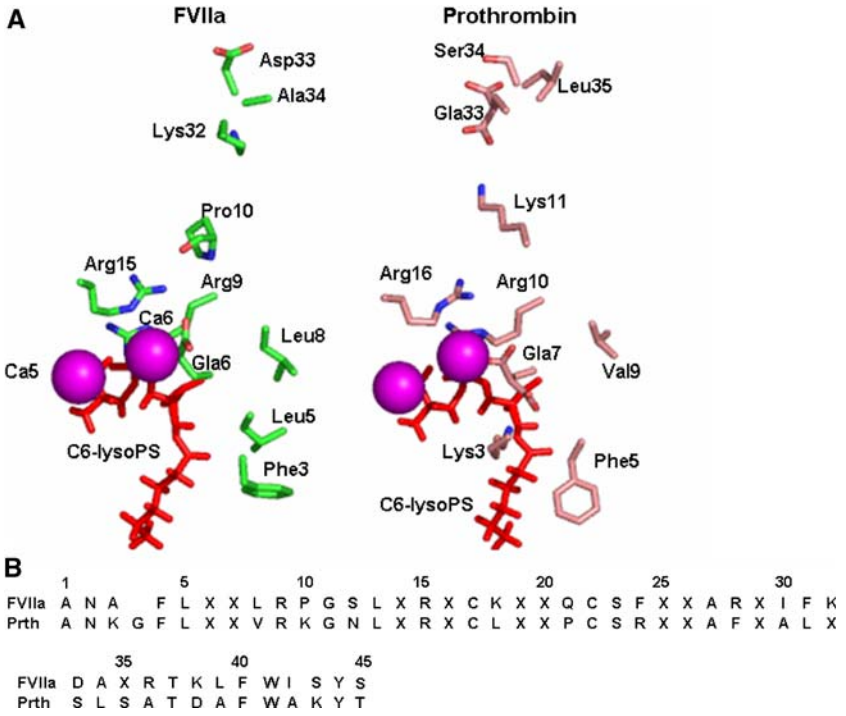

Fig. 1 **a** Structures of residues in Gla domain expected to contribute to the membrane contact. Calcium ions are shown in van der Waal (vdW) spheres in magenta, C6-lysophosphatidylserine (C6-lysoPS) in *red*. Only side chains of residues are depicted. **b** Comparison of amino acid sequences of the N-terminal Gla domains in human FVIIa and bovine Prth, with X corresponding to the Gla residue

In this context, we considered theoretical methodologies that could elucidate the role of the Gla domain and more specifically the role of the individual amino acid residues in the contribution to phospholipid membrane affinity. Based on the structure of the bovine Prth fragment 1 in complex with calcium and lysoPS, structures including human FVIIa and various FVIIa mutants complexed with calcium and lysoPS were modelled. Subsequently, molecular dynamics (MD) and steered molecular dynamics (SMD) simulations were performed on these complexes, analysed and compared to simulations on the lysoPS/Prth complex.

Steered molecular dynamics is a recent attractive approach that has already provided important qualitative insights in the dynamic and kinetic processes of ligand–receptor binding and unbinding as well as conformational changes in biomolecules on a time scale accessible to MD simulations (Isralewitz et al. 2001a, b). It allows a direct observation of the dynamics of protein–ligand interactions and can propose alternative explanations of elastic or stretching properties of proteins when experimental methods like AFM cannot be applied (Gao et al. 2002; Shen et al. 2003; Gullingsrud and Schulten 2003). In our study, the combination of MD and SMD simulations allows us to analyse the motions and the mobility of protein mutants, and provides increased understanding of the structure–function relationship of the simulated proteins. The rupture force needed to pull out the lysoPS of the different Gla domains was monitored and compared to kinetic properties of FVIIa's membrane interaction, estimated by Nelsestuen (McDonald et al. 1997; Harvey et al 2003).

Variation in the Gla6 side chain orientation (Gla7 in Prth numbering) was seen in FVIIa and Prth crystal structure. A rotation along its χ^1 angle (Cα–Cβ bond) by ~120° was observed. To elucidate in detail the conformational changes of Gla6 (Gla7 in Prth) residue in FVIIa with or without insertion of Tyr4 adiabatic mapping was applied where the two dihedral angles, χ^1 and χ^2, of the Gla6 side chain were rotated at equally spaced angular intervals from 180° to –180° in steps of 5°, while keeping the surrounding atoms fixed. The conformations identified on the basis of steric and energetic criteria were then considered. This approach confirmed that the particular orientation of Gla6 resulting from the insertion of Tyr4 in FVIIa plays a critical functional role in the binding of these proteins to membrane surfaces (Huang et al. 2004).

Methods

The starting structures of the Gla domain for the human FVIIa and the bovine prothrombin (Prth) were based on the TF/FVIIa crystal structure (protein data bank (PDB) entry 1DAN) (Banner et al. 1996) and Prth fragment 1 in complex with calcium and lysoPS (protein data bank (PDB) entry 1NL2) (Huang et al. 2003), respectively. The structure of the fragment 1–47 of FVIIa corresponding to the Gla domain was superimposed to the Prth Gla domain. All studies and analyses were applied exclusively on the Gla domains. The structure of lysoPS from the complex with Prth was superimposed to FVIIa, providing an appropriate orientation of the lysoPS/FVIIa Gla domain. The seven internal Ca^{2+} ions of FVIIa Gla domain were conserved in their respective positions from the X-ray structure. Models of FVIIa and mutants: Tyr4 insertion (FVIIa(Tyr4)), P10Q, P10Q/K32E, P10Q/D33E, P10Q/K32E/D33F, P10Q/K32E/A34E and P10Q/K32E/D33F/A34E, were prepared within InsightII (Accelrus Inc., San Diego, CA, USA).

MD simulation protocol

To limit the perturbation of the long flexible acyl chain of lysoPS during MD simulations, dicaproylphosphatidylserine (C6-lysoPS) was used. Models of proteins with Ca^{2+} and lysoPS bound were solvated with water molecules in a periodic truncated octahedron with the box boundaries at least 6.0 Å from any given protein atom. The resulting systems consisted of 47 Gla domain residues, 7 Ca^{2+}, 45 C6-lysoPS atoms and approximately 3,800 water molecules. The simulations in the present study were performed using the CHARMM22 force-field (McKerell et al. 1998) and NAMD 2.5 (Kale et al. 1999), applying an integration time step of 1 fs. The non-bonded vdW interactions were calculated with a cut-off using a switching function starting at a distance of 10 Å and reaching zero at 14 Å. A non-bonded interaction distance of 16 Å and a non-bonded energy term, with a one to four non-bonded interaction scaling factor of 1.0, were applied.

Full electrostatic interactions were treated using the particle mesh Ewald (PME) method (Darden et al. 1993; Essmann et al. 1995). To save computation time, the electrostatic forces were evaluated only every 2 fs, and the full electrostatic interaction energy every 4 fs (Cornell et al. 1995). Langevin dynamics was used to keep the temperature constant. All simulations were carried out at 300 K and a pressure of 1 atm (1 atm = 101.3 kPa) was applied in the NPT simulations. All systems were

subjected to 2,500 steps of energy minimization to remove close contacts and to relax the systems. Then, NPT simulations were performed for 1.5 ns with the coordinates saved every 500 time-steps (0.5 ps). Two MD simulations, on free FVIIa and free Prth (in the absence of C6-lysoPS), were also carried out using the conditions described above, to check if the Gla domains relax to the known X-ray crystal structures.

SMD simulation protocol

Steered molecular dynamics was used to investigate several Gla domain/C6-lysoPS complexes including Prth, FVIIa and various FVIIa mutants. We induced dissociation of C6-lysoPS from the Gla domain, applying time-dependent external forces on C6-lysoPS. A constant velocity pulling method was used with a spring constant $k = 150$ pN/Å and a velocity of 1.5×10^{-5} Å/ps. The SMD simulations started from a configuration after 500 ps of MD simulations and continued for 1.5 ns, while C6-lysoPS was pulled out from the binding pocket of the Gla domain in question. The pulling direction, corresponding to a vector direction applied along C6-lysoPS, was determined using the criterion that C6-lysoPS can pass through the putative entrance without major collisions with protein residues (mainly considering the collision with Gla6, Arg9 and Arg15 in FVIIa). The pulling potential was assigned to all the heavy atoms of C6-lysoPS and harmonic constraints were applied to Calcium 5 and Calcium 6 (corresponding to calcium 4 and calcium 6 in Prth) which interact with the two oxygens of the C6-lysoPS in FVIIa. These harmonic constraints prevent the protein from translating when external forces are applied to move C6-lysoPS in the selected direction (Israelewitz et al. 2001a, b). The force exerted along the pulling direction to pull out C6-lysoPS from the Gla domain can be expressed as $\mathbf{F} = k(vt - (\mathbf{a} - \mathbf{a}_0)\mathbf{n})\mathbf{n}$ where k is the stiffness of the spring, $\mathbf{a}_0$ the initial position of the restrain atom moving with a constant speed, v, at the time t and position $\mathbf{a}$, $\mathbf{n}$ is the unit vector in the pulling direction. The position $\mathbf{a}$ is the reaction coordinate (Israelewitz et al. 2001a, b). A schematic representation of pulling procedure is shown Fig. 2.

Adiabatic mapping

Adiabatic energy contour maps were performed to identify favourable conformations of Gla6 side chain with and without insertion of Tyrosine in position 4 of FVIIa and to compare to the adiabatic mapping of the Prth Gla7 sidechain. Dihedral angles N-Cα-Cβ-Cγ (χ^1) and Cα-Cβ-Cγ-Cd1 (χ^2) were successively rotated in steps of 5° from 180° to –180°, with a dihedral harmonic constraint (a barrier height of 1,000 kcal/mol was used). Then, each conformation generated from the same starting structure was subjected to 500 steps of Powell algorithm minimization. Energies were calculated with a 13.5 Å cut-off radius for the non-bonded interactions and all the calculations were done using a distance-dependent dielectric constant to take into account implicitly the effect of the solvent (Brook et al. 1983). All the adiabatic calculations were performed using the CHARMM22 molecular modelling package and the contour maps were drawn with Gnuplot (http://www.cs.dartmounth.edu/gnuplot_info.html).

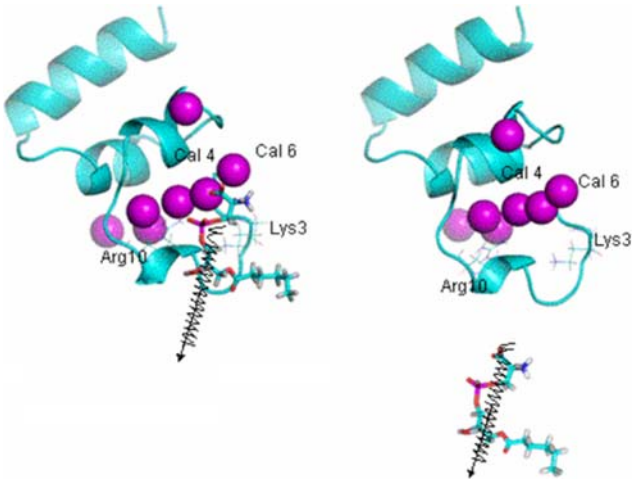

Fig. 2 A schematic representation of the SMD simulation system. The Gla domain of Prth is shown in *solid ribbon*, calcium ions in vdW spheres and C6-lysoPS in *stick representation*. C6-lysoPS is pulled away from the binding sites Ca-4 and Ca-6 using a harmonic potential symbolized by an artificial spring that is connected to the heavy atoms

Results

The conformation of Gla6 in FVIIa

The energy of FVIIa's Gla domain with different Gla6 side chain conformations was investigated and compared to the energy of Prth and FVIIa(Tyr4) with different Gla7 side chain conformations using adiabatic mapping. The resulting adiabatic energy contour map is shown in Fig. 3. The adiabatic map of FVIIa shows one energy minimum at approximately $\chi^1 = 180°$, $\chi^2 = -120°$, coresponding to the position found in the crystal structure (1DAN). The adiabatic map of Prth

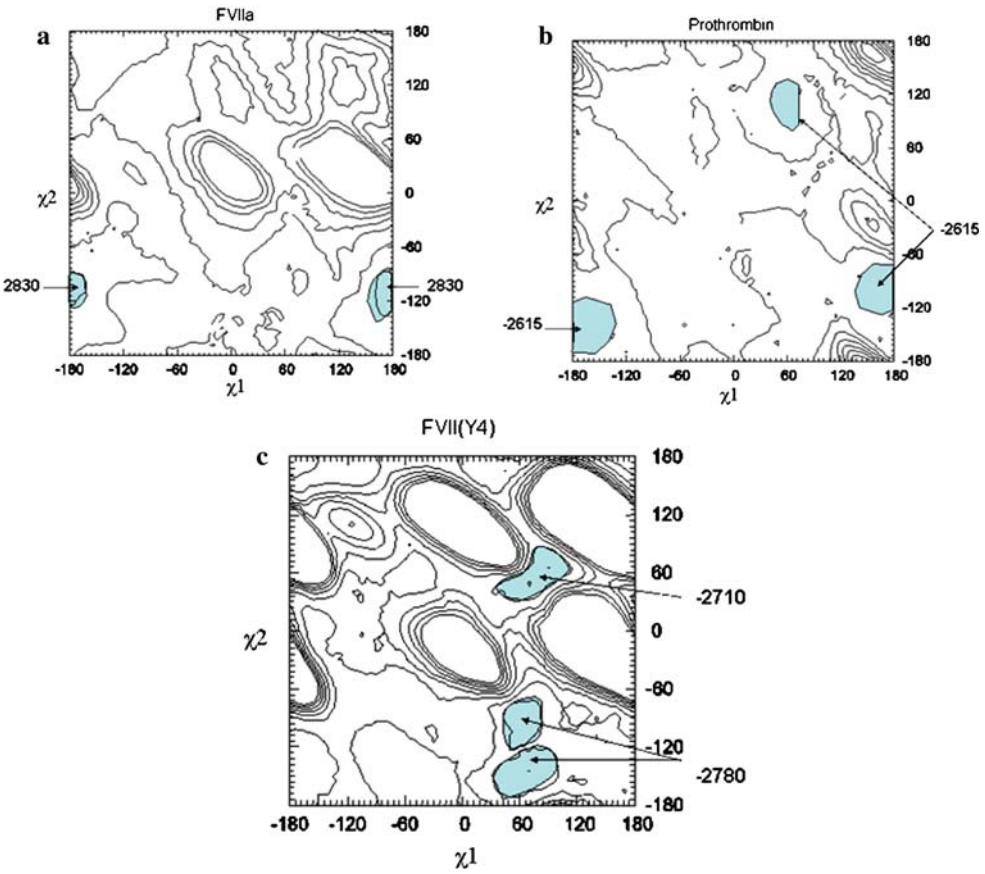

Fig. 3 Adiabatic energy contour maps for the rotation of Gla6 side chain in FVIIa (**a**), and the rotation of Gla7 side chain in Prth (**b**) and in FVIIa(Y4) insertion (**c**). The contour levels are separated by 50 kcal/mol. Energies represent the total energy of the proteins resulting from side chain rotation after minimization and are in units of kcal/mol

without PS shows two energy minima. The region $\chi^1 = 50°–70°$ and $\chi^2 = 90°–130°$ corresponds to the position found in the crystal structure (1NL2). The second region around $\chi^1 = 180°$ and $\chi^2 = –120°$ places the Gla residue in the same position as found in the FVIIa crystal structure. Due to its ω-loop, bovine Prth fragment I could adopt two conformations: one, where a carboxylate group of the Gla side chain interacts with calcium ions 4 and 5 (Ca–4 and Ca-5); the other carboxylate group forms hydrogen bonds to the main chain nitrogen atoms of Lys3, Gly4 and Phe5 (Prth numbering). The second conformation orients the side chain in the same position as in FVIIa where both of the carboxylate groups of the Gla side chain bridges Ca-4 and Ca-5. To examine if the difference in orientation is a result of the Tyrosine insertion in Prth's N-terminal sequence, an adiabatic map was done on FVIIa(Y4). An energy minimum is located in the same region as shown in the Prth map ($\chi^1 = 40°–90°$ and $\chi^2 = 50°–90°$). Two other regions are observed as a result of the χ^2 rotation ($\chi^2 = –100°$ and $\chi^2 = –160°$). In these regions one or the other carboxylate group can interact with Ca-4 and Ca-5. The rotation of this Gla side chain seems partly related to the insertion of one residue in position 4. The main chain nitrogen atom makes hydrogen bonds with the carboxylate group of the Gla residue and stabilizes the ω-loop in a specific conformation (Fig. 4).

MD simulations

Molecular dynamics simulations on the Gla domains of Prth, FVIIa, FVIIa(Y4), P10Q, P10Q/K32E, P10Q/A34E, P10Q/D33F, P10Q/K32E/D33F, P10Q/K32E/A34E and P10Q/K32E/D33F/A34E, all in complex with C6-lysoPS, as well as two controls, were carried out for 1.5 ns. Several time-dependent properties were analysed to examine the stability of the MD simulations. To describe the mobility, the root-mean-square deviation (rmsd) of the main chain atoms, with respect to the starting structure, was evaluated during the simulations (Fig. 5a). For clarity we discuss results from simulations on Prth, FVIIa, FVIIa(Y4), P10Q and P10Q/K32E in details and comment on results from the last three mutants.

The free FVIIa system (without C6-lysoPS) is stable and stays close to the FVIIa X-ray structure (1DAN). The insertion of a C6-lysoPS in FVIIa does

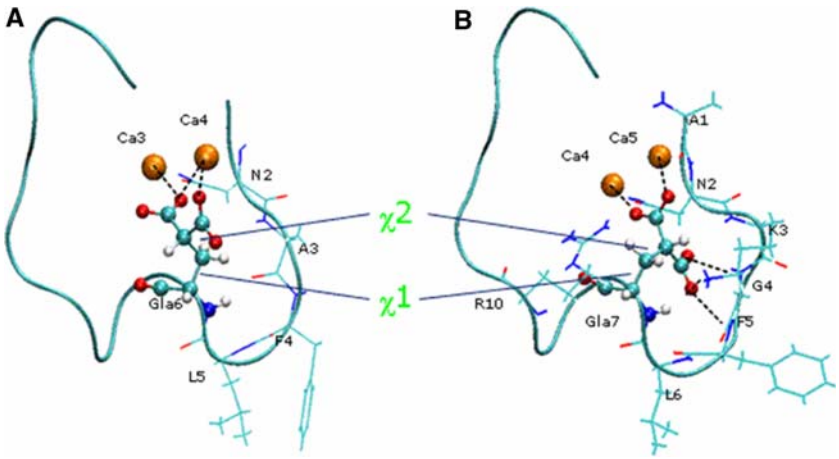

Fig. 4 Differences in conformation of Gla-6 residue in FVIIa (**a**) and Prth (**b**). Hydrogen bonds of Gla-6 and interaction with calcium in ω-loop are shown in *dash*. Both of the dihedral angles χ^1 and χ^2 being rotated during the adiabatic process are *marked*

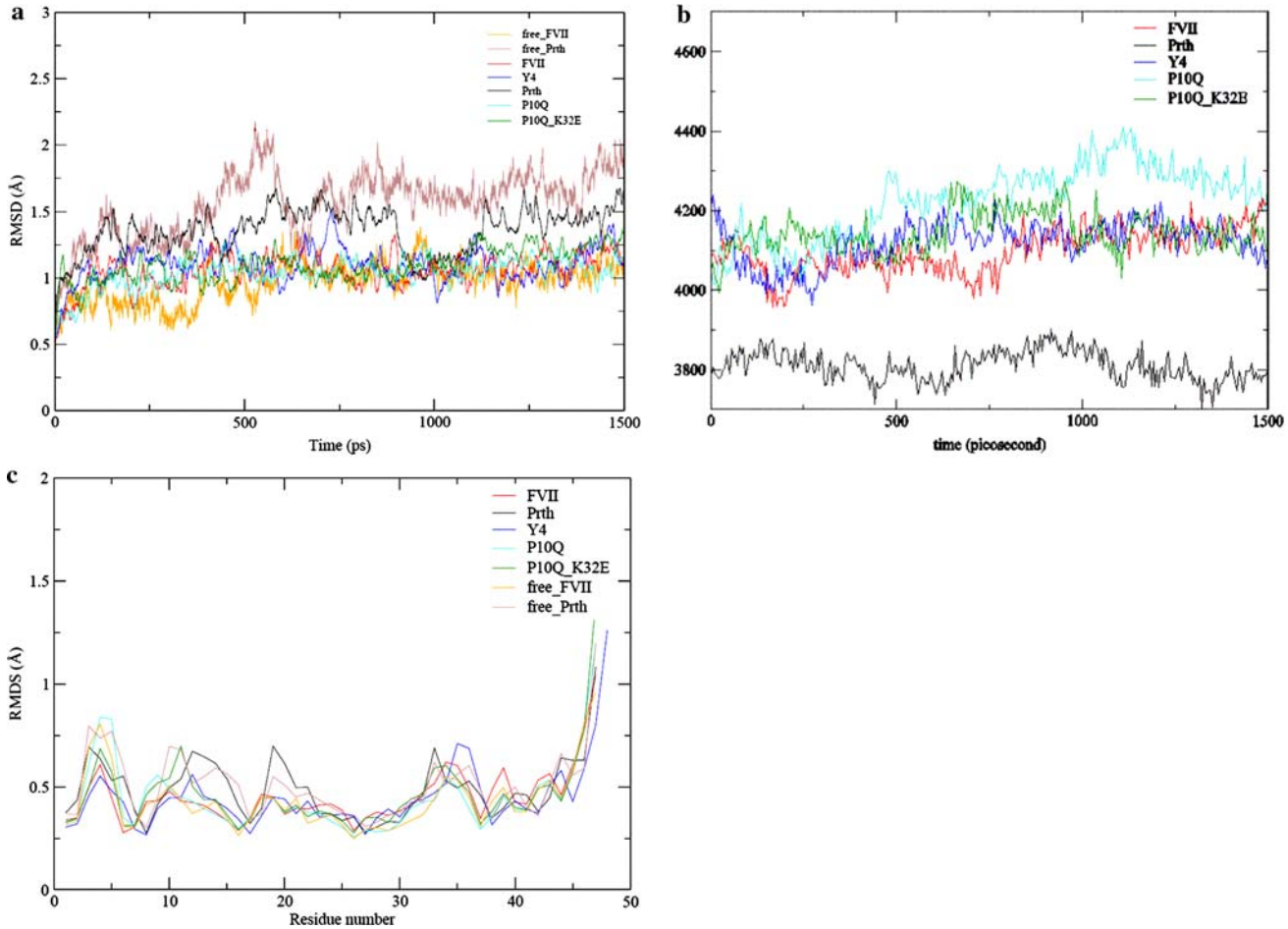

Fig. 5 **a** Root-mean-square deviations (rmsds) of main chain atoms calculated along the trajectories. The main chain atoms of first 47 residues in each configuration are used for optimal alignment with those of the FVIIa and Prth X-ray structure. **b** Total accessible surface area (ASA) of Prth and FVIIa fragments (Gla domains) along the trajectories. **c** Root-mean-square deviation (rmsd) of the Cα atoms calculated for the last 500 ps

not perturb the system, as the RMS looks as stable as that of free FVIIa. The free Prth is more perturbed in the absence of C6-lysoPS. The lack of contacts between C6-lysoPS and the ω-loop forces the molecule into a changed configuration. Nevertheless, the structure becomes stable along the simulation and approaches the X-ray structure of free Prth (1NL2).

During the first 150 ps the systems relax and close contacts are removed. Then, the systems are relatively stable, except for Prth (with and without C6-lysoPS) which shows larger fluctuations in the RMS displacement, indicating an inherent global flexibility compared to FVIIa. The mobility of the FVIIa models is somewhat smaller than that of Prth. Even the insertion of Tyr4 into FVIIa does not generate a high mobility of the protein. In addition, the total accessible surface area (ASA) (Fig. 5b) suggests that structures related to FVIIa are less compact and more solvent-exposed than that of the Prth structure. The insertion of Tyr4 reduces slightly the exposure of the protein to the solvent and stabilizes the conformation. So, despite the higher flexibility of Prth compared to FVIIa fragments, the trajectories are stable. Moreover, nearly constant total accessible surface area suggests that the Gla domains, in the presence of C6-lysoPS and calcium, are in dynamic but stable conformations.

To further evaluate the dynamics, the rmsd of the main chain atoms from residues 1–47 over the last 500 ps of each trajectory were calculated (Fig. 5c). The last two residues display large rmsd, superior to 1 Å, for all simulations, which are expected for the free C-terminus. The rest of the Gla domain is relatively stable with an rmsd around 0.5 Å. The larger displacements occur essentially in the ω-loop with mobility of residues 3, 4, 5 and around positions 10 and 32. It is interesting to note, that mutations in these positions do not perturb the conformations. Only, Prth shows a fluctuation around Leu19 and Gla20 compared to FVIIa proteins. These residues form an α-helix that seems to be stretched during the simulation. The seven calcium ions are also very stable with a displacement less than 0.60 Å due to the network with Gla residues (Table 1).

The motion of C6-lysoPS along the different trajectories was also investigated. Firstly, to validate the force field implemented for C6-lysoPS in the simulation, the stability of C6-lysoPS with Prth was analysed and compared to the X-ray structure. The binding of the carboxyl oxygen of the C6-lysoPS head group to Ca-5 and Ca-6 was preserved along the simulation. Hydrogen bonds between NH1 of Arg9 and NH1 of Arg15 with terminal phosphate oxygen of C6-lysoPS were quite conserved (present 92 and 32% of the time, respectively). However, the salt bridge and hydrogen bond between Lys3 and the glycerol phosphate were broken after 300 ps. Nevertheless, hydrophobic contacts are still present with Lys3 and also with Phe4, Leu5 and Gla6, keeping C6-lysoPS relatively stable and with the same features as observed in the crystal structure.

Table 1 Calcium interaction with Gla residues in FVIIa and prothrombin along the 1.5 ns trajectory

FVIIa		Prth	
Ca-1	Gla29-OE4 (96%) Gla7-OE1 (92%) Gla25-OE2 (10%) Gla25-OE3 (2%)	Ca-1	Gla30-OE2 (27%) Gla26-OE1 (5%)
Ca-2	Gla6-OE2 (57%) Gla26-OE2 (16%) Gla26-OE4 (13%)	Ca-2	Gla27-OE1 (86%) Gla8-OE3 (18%) Gla30-OE4 (15%) Gla8-OE1 (10%)
Ca-3	Gla16-OE2 (96%) Gla26-OE1 (91%) Gla26-OE3 (8%) Gla16-OE4 (8%)	Ca-3	Gla30-OE4 (84%) Gla27-OE4 (38%) Gla27-OE2 (25%)
Ca-4	Gla6-OE2 (79%) Gla6-OE3 (26%)	Ca-4	Gla27-OE1 (86%) Gla17-OE4 (55%) Gla17-OE2 (4%)
Ca-5	Gla14-OE4 (15%) Gla19-OE1 (3%)	Ca-5	Gla7-OE1 (68%)
Ca-6	Gla19-OE2 (94%) Gla20-OE2 (9%)	Ca-6	Gla20-OE1 (90%)
Ca-7	Gla25-OE4 (38%) Gla29-OE2 (35%)	Ca-7	Gla15-OE1 (10%) Gla20-OE4 (8%)

The values in parentheses correspond to the % of time bond along the molecular dynamics (MD) simulation

For FVIIa, the contact between carboxyl oxygen of C6-lysoPS and Ca-4 is already lost in the preliminary step of the trajectory. In fact, during the minimization procedure, a rearrangement of C6-lysoPS occurs and both Ca-4 and Ca-6 bind to the same carboxyl oxygen. The loss of this contact can be explained by the missing hydrogen bond between the serine carboxyl oxygen and the carboxyl oxygen of Gla16. The hbond network becomes weak and destabilizes the bridge between the serine carboxyl oxygen and Ca-4. During the simulation Arg9 (NH1) forms a hydrogen bond to the terminal phosphate oxygen (O51). Another hydrogen bond between phosphate oxygen (O51) and Arg15 (NH1), seen in Prth, is missing in FVIIa. The particular orientation of Gla6 side chain seems to be the explanation for the missing interaction due to repulsion with the glycerol phosphate oxygen resulting in a rotation of the phosphatidyl chain. Despite these perturbations, hydrophobic contacts are still present with Phe4, Leu5 and Gla6.The insertion of Tyr4 in FVIIa results in the same rearrangement i.e. only binding of one carboxyl oxygen to both calcium Ca-4 and Ca-6, and a missing hydrogen bond between the serine carboxyl oxygen and the carboxyl oxygen of Gla17. However, both hydrogen bonds between Arg9 and Arg15 with the terminal phosphate oxygen are conserved during the simulation, resulting in a Gla6 orientation which stabilizes the phosphatidyl chain. The glycerophosphate

main chain conserves some hydrophobic contacts with Leu5 and Gla6. In contrast, Phe4 has no role in stabilization of C6-lysoPS due to lack of contact.

Finally, the mutated side chains in the mutations P10Q and P10Q/K32E are not in close contact with C6-lysoPS. In both simulations, the calcium interaction to the carboxyl oxygen of the serine head group is conserved as well as the hydrogen bonds with carboxyl oxygen of Gla16 and Gla20. However, hydrogen bonds to Arg9 are lost and very intermittent with Arg15. The P10Q mutation generated new hydrogen bonds with Gly11 and Gla29, with a rotation of 13° of the Gly11 main chain. This rearrangement generates more mobility of Arg9. As seen for the K32E mutation, mobility also appears for Arg28 and Arg36. K32E is close to Gln10, but the hydrogen bond is not stable (only present 4% of the time). Most of the hydrophobic contacts between C6-lysoPS and the solvent exposed residues are also lost. All these results are further depicted in Fig. 6. The same arrangements are seen in the last four simulated mutants.

SMD simulations

The rupture force-profile derived from SMD simulations are compared in Table 2. The Prth/C6-lysoPS complex exhibits the largest resistance to external forces when the complex dissociates after 1.7 ns of SMD simulation with a force of 1,597 pN whereas the FVIIa/C6-lysoPS complex dissociates at 1.13 ns with a rupture force of 728 pN. Simulations on the complexes of Y4, P10Q and P10Q/K32E, and C6-lysoPS show intermediate rupture forces of 765, 1,036 and 1,194 pN at 1.36, 1.43 and 1.55 ns, respectively. These rupture forces reflect the binding affinity determined experimentally (Harvey et al. 2003; Zhang and Castellino 1993). The main interactions disrupted by the external forces are the calcium bridges with the serine carboxyl oxygen of C6-lysoPS. The rupture force in Prth, P10Q and P10Q/K32E corresponds to the dissociation of one Ca^{2+} with one carboxyl oxygen followed rapidly by the rupture of the second Ca^{2+} with the other carboxyl oxygen. It is interesting that the hydrogen bond be-

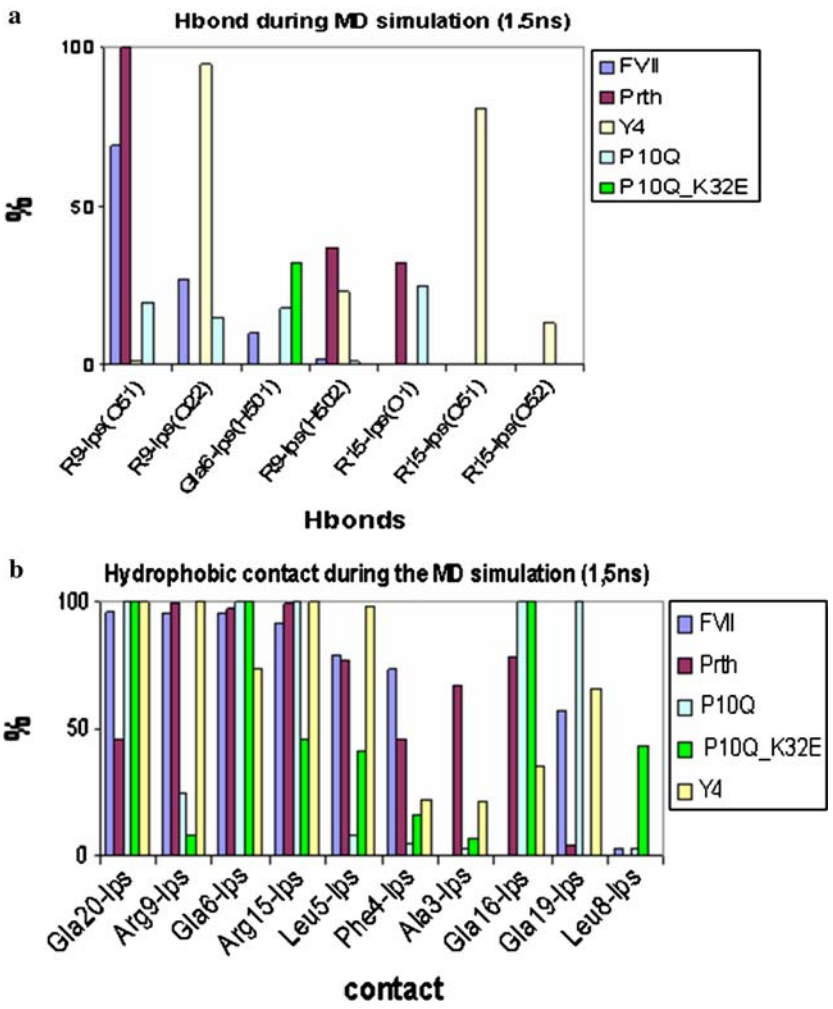

Fig. 6 Hydrogen bonds (**a**) and hydrophobic contact (**b**) between C6-lysoPS and residues of the Gla domain, along the trajectory (1.5 ns) are defined in percent

Table 2 Rupture force necessary to dissociate C6-lysoPS

	Rupture force (pN)	Time (ns)	K_d (μM)
FVIIa	728	1.13	5.8
Y4	750	1.36	2.9
P10Q	1,036	1.43	3.2
P10Q/K32E	1,194	1.55	0.16
P10Q/D33E	1,157	1.49	0.48
P10Q/K32E/D33F	1,534	1.71	
P10Q/K32E/A34E	1,442	1.70	0.12[a]
P10Q/K32E/D33F/A34E	1,307	1.58	0.05[a]
Prth	1,597	1.70	0.037[a]

K_d measurements are from Harvey et al. 2003

[a] An estimation from McDonald et al.(1997)

tween Lys3(HZ2) and PS(O51) in Prth is strongly preserved until the dissociation (i.e. present 79% of the time). The side chains of Lys3 and Arg9 form a canal that seems to have an important role in stabilizing the C6-lysoPS binding. In the complexes of P10Q and P10Q/K32E as well as FVIIa with C6-lysoPS, the missing interaction with the side chain of Lys3 seems to be partially compensated by a contact between carboxyl oxygen of the Gla6 residue and the nitrogen of the serine phosphate. However, the hydrogen bond is only partially stable (present in less than 15% of the time in the three cases). The SMD simulation on the Tyr4/C6-lysoPS complex exhibits a loss of one calcium–carboxyl oxygen interaction very early during the simulation (0.75 ns). A second peak in the rupture force appears after 1.14 ns. At this point, two strong hydrogen bonds between Arg15 and C6-lysoPS (O51) and (O52) are lost followed by the unbinding of carbonyl oxygen to Ca^{2+} at 1.36 ns. Finally, the simulation on the FVIIa/C6-lysoPS complex shows two distinct peaks at 1.04 and 1.13 ns. At the beginning of the simulation, both carboxyl oxygens of C6-lysoPS, interact with one Ca^{2+}. At the first peak, one interaction with Ca^{2+} is lost, and at the second peak the other interaction is lost. The interaction of C6-lysoPS with only one calcium ion seems to weaken the binding affinity (Fig. 7). An investigation of the impact of the pulling velocity was also carried out. Previous work has indicated that the higher the velocity, the higher force is needed to unbind a substrate or unfold a protein (Shen et al. 2003). Non-equilibrium effects can be introduced at a high pulling velocity and lead to artefacts in the simulations. Therefore, we also performed SMD simulations on all nine Gla domain protein/C6-lysoPS complexes using a different pulling velocity (1.5×10^{-4} Å/ps). At a ten times higher pulling velocity, the global shapes of the force profiles are similar with a higher force needed in a shorter time (data not shown). So the pulling velocity (in the present range) should not affect the unbinding process of C6-lysoPS. A second point to consider in SMD simulations is the pulling direction used during the unbinding process. How can we be sure that the chosen path does not produce artefacts? In our study the direction of the force was chosen as a straight-line path in an attempt to avoid collisions with protein residues. Izrailev et al. (1998) suggest defining a conical region of space around a preferred direction and selecting new directions randomly within this region. In order to test the robustness of the present approach we performed a

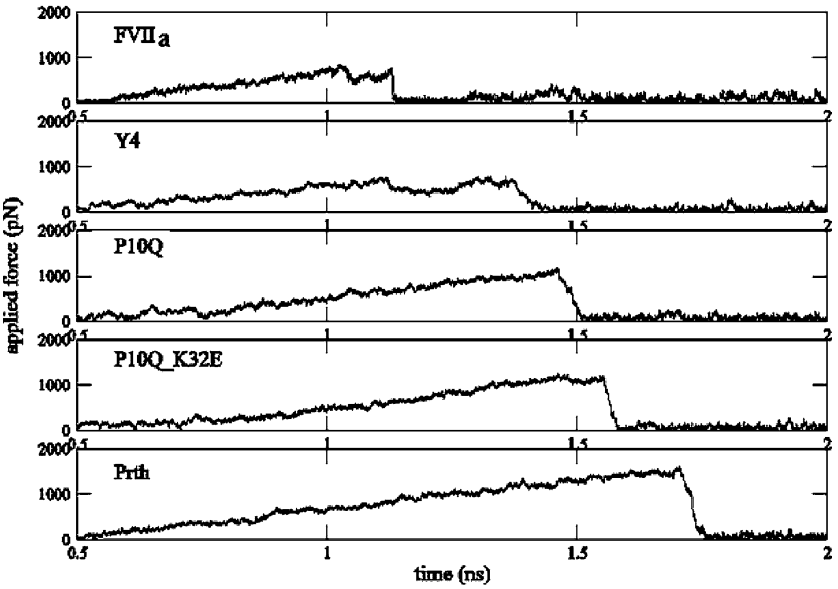

Fig. 7 Rupture force exerted on Gla domain during C6-lysoPS dissociation versus simulation time at a pulling velocity of 1.5×10^{-5} Å/ps and with a spring constant $k = 150$

second SMD simulation applying a different direction of the force for FVIIa and Prth. Results are quite similar with a rupture force of 600 and 1,900 pN for FVIIa and Prth, respectively, which suggest that a straight-line path is sufficient to unbind C6-lysoPS without major artefacts.

Discussion

The nature of the membrane contact site in vitamin-K-dependent proteins is still unclear and evidence of critical residues of the Gla domain is rather limited. Previous studies have shown that Gla residue replacement with Asp in human Prth and factor X resulted in loss of function for Gla17, Gla27 and Gla30 (Ratcliffe et al. 1993; Larson et al. 1998). In all our MD simulations, binding of these Gla residues to calcium ions are conserved along the trajectories and, at least one oxygen of both carboxyl oxygen participates in the interaction with a calcium ion (Table 1). Consequently, mutations of these Gla residues to Asp reduce the calcium ionic contact and may destabilize the protein conformation. Mutation of the other Gla residues (Gla7, Gla8, Gla15, Gla17, Gla20, Gla21 and Gla26 in Prth) to Asp has a weaker impact on the binding affinity and is probably due to the notion that only one carbonyl oxygen is necessary to bind the calcium. The carboxylate group of Asp can fully play this role.

In the adiabatic mapping experiment, we showed that the low energy orientations of Gla6 side chain are influenced by the insertion (Prth) or no insertion (FVIIa) of an amino acid after position 3. These specific orientations are similar in Factor Xa (16) (no insertion) and Factor IXa (Shikamoto et al. 2003) (insertion) and display the same structural features as in FVIIa and Prth, respectively. The low energy conformation of the Gla7 side chain in Prth generates a hydrogen bond network more potent and more strongly conserved than in FVIIa during MD simulations. We also investigated the impact of Gla6 residue of wild type FVIIa in the same side chain orientation as in Prth and without any residue insertion. Clashes with Ala3 main chain appeared and minimization generated a rotation of ~180° of its main chain oxygen with small reorganizations of the five N-terminal residues. But the hydrogen bond network of the amine of Ala1 with Gla26 and Gla16 and Asn2 with Gla26 still kept the N-terminal buried in the folded structure (data not shown), affording the N-terminus protection from acetylation (Giannelli and Green 1993). In addition, the ω-loop is as stable as in the FVIIa (Y4) mutant during MD simulation suggesting it is essentially a steric problem that prevents an orientation of Gla6 residue like the one observed in Prth. In relation to this observation it is interesting to notice the presence of a lysine in position 3 of Prth and position 5 of FIX, respectively. Previous investigations have shown that lysine in these positions play a major role in the phosphatidyl serine binding (Grant et al. 2004; Huang et al. 2004). However, Factor X with no insertion and no lysine in this region was shown to have a membrane binding affinity just as potent as bovine Prth I and even better than FIXa (McDonald et al. 1997). Our MD simulations show, that the specific Gla6 side chain orientation in FVIIa, P10Q and P10Q/K32E participates in the anchoring of C6-lysoPS via hydrogen bond between carboxyl oxygen of Gla6 and nitrogen hydrogen of phosphatidyl serine. This interaction is not present in Prth and FVIIa (Y4). So, the orientation of the Gla6 side chain in FVIIa and FXa may have a compensating role in the membrane binding in the absence of G4 or Y4 insertion and lack of neighbouring lysine.

In any case, these data are in agreement with previous observations that showed the phosphatidylserine specificity of Prth binding to phospholipid membranes (Lu and Nelsestuen 1996). With the modification of the phospholipids head group to an ethanolamine or choline, the electrostatic interaction with the Gla domain become unfavourable, especially with the calcium, Gla16 and Gla20 and Gla6 in FVIIa.

To investigate the Gla/C6-lysoPS complex further, MD and SMD simulations were also undertaken. According to the crystal structure of the complex Prth/C6-lysoPS and previous experimental studies, the role is evident of the hydrophobic patch formed with Phe4, Leu5 and Val8, and Ca-4 and Ca-6 in Prth for the contribution of the membrane binding. The role of P10 and K32 is less well documented. The P10Q and K32E mutations are relatively far from C6-lysoPS in FVIIa to have a direct contribution (around 6.5 and 15 Å, respectively). Nevertheless, coupling of these mutations has a strong impact on the membrane-binding affinity possibly resulting from reorganization of the Gla domain. The rotation of the Gly11 main chain generated during the MD simulation, to form a hydrogen bond with Q10 side chain as well as the appearance of a hydrogen bond between E32 and Q10 force the loop harbouring Arg9 and Arg15 to shrink and may so enhance the accessibility of the phospholipids to the calcium ions. In a previous study additional mutations H10Q and S11G on protein C required lower calcium concentration for membrane association but with nearly identical membrane-binding affinity at saturating calcium levels. It was

concluded that these mutations modify calcium binding to the protein without participation in actual membrane contact (Shen et al. 1998; Izrailev et al. 1998). With MD and SMD approaches, we arrive at the same conclusion. For mutations containing the P10Q and K32E, new interactions will in a first step stabilize the Gla domain and then facilitate accessibility to the calcium ions, increasing affinity for calcium binding. Now, to further evaluate the applicability of the SMD approach a series of four MD and SMD simulations involving P10Q/D33E, P10Q/K32E/D33F, P10Q/K32E/A34E and P10Q/K32/D33F/A34E were also performed. Even though their binding affinities were not explicitly described, the impact of the mutations D33F and A34E in association with P10Q/K32E was evaluated previously (Harvey et al 2003). So, for example the introduction of D33F increased the membrane affinity of P10Q/K32E by 2-fold whereas A34E showed a 1.5-fold increase in affinity when introduced into P10Q/K32E/D33F. Based on our SMD simulations, P10Q/K32E/D33F and P10Q/K32E/A34E showed a rupture force of 1,534 pN at 1.71 ns and 1,442 pN at 1.70 ns, respectively (see Table 2). The introduction of D33F or A34E into P10Q/K32E enhance the binding affinity for C6-lysoPS in agreement with the experimental data. In the structures, D33F and A34E are quite far from P10Q (15 and 12 Å) and no interactions were clearly observed between both mutations and P10Q. Instead Glu34 has an ionic interaction with Arg28 and Phe33 placed between Glu32 and Gla36. Additionally, the SMD simulation of the four mutations in combination (P10Q/K32E/D33F/A34E) shows a rupture force of 1,307 pN. This result does not match with the experimental observation.

It was suggested previously that the mutation to a Glu in positions 32 and 34 can be modified to a Gla during the post-translational carboxylation and so could have a direct role for this region in membrane association whereas addition of a large hydrophobic side chain in this vicinity (like the D33F) may serve to isolate this charge complex from water molecules. A second hydrophilic patch identified in the surface of the cavity surrounded by Gla29, Gla7 and Gla32 in Prth has been proposed to be essential for membrane binding (Harvey et al. 2003; Mizuno et al. 2001). Calcium 1 would participate in a binding interaction with the negatively charged head group on the membrane surface and Gla32 with a potential for calcium ion binding. So, the combination of mutations might generate a second PS-binding site, which is not taken into account in the present study.

In conclusion, SMD simulations were used in an effort to interpret the effects of mutagenesis in FVIIa in terms of binding affinity. This method provides an atomic level description of phosphatidylserine interactions with Gla domain according to specific mutations and how some residues of the Gla domain, can participate in a direct or indirect manner to the membrane binding. Most of residues from the ω-loop have an important role in the protein stability and accessibility to the phospholipid membrane. Furthermore, the relevant, ionic interactions with calcium, hydrogen bonds network and hydrophobic interactions with the phosphatidylserine emphasize the protein/lysoPS complex stability.

References

Banner DW, Arcy A, Chen C, Winkler FK, Guha A, Konigsberg WH, Nemerson Y, Kirchofer D (1996) The crystal structure of the complex of blood coagulation factor VIIa with soluble tissue factor. Nature 380:41–46

Brook BR, Bruccoleri RE, Olafsen BD, States DJ, Swaminthan S, Karplus M (1983) CHARMM: a program fro macromolecular energy, minimization and dynamics calculations. J CompChem 4:187–217

Christiansen WT, Jalbert LR, Robertson RM, Jhingan A, Prorok M, castellino FJ (1995) Hydrophobic amino acid residues of human anticoagulation protein C that contribute to its functional binding to phospholipids vesicles. Biochemistry 34:10376–10382

Cornell WD, Coeplak P, Bayly CI, Gould IR, Merz KM, Ferguson DM, Spellmeyer DC, Fox T, Caldwell JW, Kollman PA (1995) A 2nd generation force field for the simulation of proteins, nucleic-acids, and organic-molecules. J Am Chem Soc 117:5179–5197

Davie EW, Fujikawa K, Kisiel W (1991) The coagulation cascade: initiation, maintenance, and regulation. Biochemistry 30:10363–10370

Darden T, York D, Pedersen L (1993) Particle mesh Ewald: an *N*-log(*N*) method for Ewald sums in large systems. J Chem Phys 98:10089–10092

Essmann U, Perera L, Verkowitz ML Darden T, Lee H, Pedersen LG (1995) A smooth particle mesh Ewald method. J Chem Phys 103:8577–8592

Falls LA, Furie BC, Jacobs M, Furie B, Rigby AC (2001) The ω-loop region of the human prothrombin γ-carboxyglutamic acid domain penetrates anionic phospholipd membranes. J Biol Chem 276:23895–23902

Fetrow S (1995) Omega loops: nonregular secondary structures significant in protein function and stability. FASEB J 9:708–717

Freedman SJ, Blostein MD, Baleja JD, Jacobs M, Furie BC, Furie B (1996) Identification of the phospholipid binding site in the vitamin K-dependent blood coagulation protein factor IX. J Biol Chem 271:16227–16236

Furie B, Furie BC (1988) The molecular basis of blood coagulation. Cell 53:505–518

Furie B, Furie BC (1992) Molecular and cellular biology of blood coagulation. New Engl J Med 326:800–806

Gao M, Lu H, Schulten K (2002) Unfolding of titin domains studied by molecular dynamics simulations. J Mus Res Cell Mot 23:513–521

Giannelli F, Green P (1993) Haemophilia B: database of point mutations and short additions and deletions. Nucleic acids Res 21:3075–3087

Grant MA, Baikeev RF, Gilbert GE, Rigby AC (2004) Lysine 5 and Phenylalanine 9 of the Factor IX ω-loop interact with phosphatidylserine in a membrane mimic environment. Biochemistry 43:15367–15378

Gullingsrud J, Schulten K (2003) Gating of MscL studied by steered molecular dynamics. Biophys J 85:2087–2099

Harvey SB, Stone MD, Martinez MB, Nelsestuen GL (2003) Mutagenesis of the γ-Carboxyglutamic acid domain of human factor VII to generate maximum enhancement of the membrane contact site. J Biol Chem 278:8363–8369

Huang M, Rigby AC, Morelly X, Grant M, Huang G, Furie B, Seaton B, Furie BC (2003) Structural basis of membrane binding by Gla domains of vitamin K-dependent proteins. Nat Struct Biol 10:751–756

Huang M, Furie BC, Furie B (2004) Crystal structure of the calcium-stabilized Human factor IX Gla domain bound to a conformation-specific anti-factor IX antibody. J Biol Chem 279:14338–14346

Izrailev S, Stepaniants S, Isralewitz B, Kosztin D, Lu H, Molnar F, Wriggers W, Schulten K (1998) Steered molecular dynamics. In: Deuflhard P, Hermans J, Leimkuhler B, Mark AE, Reich S, Skeel RD (eds) Computational molecular dynamics: challenges, methods, ideas. Lecture notes in computational science and engineering, vol 4. Springer, Berlin Heidelberg New York, pp 39–65

Isralewitz B, Baudry J, Gullingsrud J, Kosztin D, Schulten K (2001a) Steered molecular dynamics investigations of protein function. J Mol Model 19:13–25

Isralewitz B, Gao M, Schulten K (2001b) Steered molecular dynamics and mechanical functions of proteins. Curr Opin Struct Biol 11:224–230

Kale L, Skeel R, Bhandarkar M, Brunner R, Gursoy A, Krawetz N, Phillips J, Shinozaki A, Varadarajan K, Schulten K (1999) NAMD2: greater scalability for parallel molecular dynamics. J Comp Phys 151:283–312

Larson PJ, Camire RM, Wong D, Fasano NC, Monroe DM, Tracy PB, High KA (1998) Structure/function analyses of recombinant variants of human factor Xa: Factor Xa incorporation into prothrombinase on the thrombin-activated platelet surface is not mimicked by synthetic phospholipd vesicles. Biochemistry 37:5029–5038

Lu Y, Nelsestuen GL (1996) Dynamic Features of Prothrombin interaction with phospholipids vesicles of different size and composition: implication for protein-membrane contact. Biochemistry 35:8193–8200

Magnusson S, Sottrup-Jensen L, Peterson TE, Morris HR, Dell A (1974) Primary structure of the vitamin K-dependent part of prothrombin. FEBS Lett 44:189–193

McDonald JF, Shah AM, Schwalbe RA, Kisiel W, Dahlback B, Nelsestuen GL (1997) Comparison of Naturally occurring vitamin K-dependent proteins: correlation of amino acid sequences and membrane binding properties suggests a membrane contact site. Biochemistry 36:5120–5127

McKerell AD Jr, Bashford D, Bellott M, Dunbrack RL Jr, Evanseck J, Field MJ, Fisher S, Gao J, Guo H, Ha S, Joseph D, Kuchnir L, Kuczera K, Lau FTK, Mattos C, Michnick S, Ngo T, Nguyen DT, Prodhom B, Reiher IWE, Roux B, Schlenkrich M, Smith J, Stote R, Straub J, Watanabe M, Wiorkiewicz-Kuczera J, Yin D, Karplus M (1998) All-hydrogen empirical potential for molecular modelling and dynamics studies of proteins using the CHARMM22 force field. J Phys Chem 102:3586–3616

Mizuno H, Fujimoto Z, Atoda H, Morita (2001) Crystal structure of an anticoagulant protein in complex with the Gla domain of factor X. PNAS 98:7230–7234

Nelsestuen GL (1999) Enhancement of vitamin-K-dependent protein function by modification of the γ-carboxyglutamoc acid domain: study of protein C and factor VII. Trends Cardiovasc Med 9:162–167

Nelsestuen GL, Zytokovicz TH, Howard JB (1974) The mode of action of vitamin K. Identification of gamma-carboxyglutamic acid as a component of prothrombin. J Biol Chem 249:6347–6350

Nelsestuen GL, Stone M, Martinez MB, Harvey SB, Foster D, Kisiel W (2001) Elevated function of blood clotting factor VIIa mutants that have enhanced affinity for membranes. Behaviour in a diffusion-limited reaction. J Biol Chem 276:39825–39831

Ratcliffe JV, Furie B, Furie BC (1993) The importance of specific gamma-carboxyglutamic acid residues in prothrombin. Evaluation by site-specific mutagenesis. J Biol Chem 268:24339–24345

Shah AM, Kisiel W, Foster DC, Nelsestuen GL (1998) Manipulation of the membrane binding site of vitamin K-dependent proteins: enhanced biological function of human factor VII. Proc Natl Acad Sci USA 95:4229–4234

Shen L, Shah AM, Dahlback B, Nelsestuen GL (1997) Enhancing the activity of protein C by mutagenesis to improve the membrane-binding site: Studies related to Proline-10. Biochemistry 36:16025–16031

Stenflo J (1974) Vitamin K and the biosynthesis of prothrombin. IV. Isolation of peptides containing prosthetic groups from normal prothrombin and the corresponding peptides from dicoumarol-induced prothrombin. J Biol Chem 249:5527–5535

Shen L, Shal AM, Dahlbäck B, Nelsestuen GL (1998) Enhancement of human protein C function by site-directed mutagenesis of the γ-carboxyglutamic acid domain. J Biol Chem 273:31086–31091

Shen L, Shen J, Luo X, Cheng F, Xu Y, Chem K, Arnold E, Ding J, Jiang H (2003) Steered molecular dynamics simulation on the binding of NNRTI to HIV-1 RT. Biophys J 84:3547–3563

Shikamoto Y, Morita T, Fujimoto Z, Mizuno H (2003) Crystal structure of $Mg2^+$ and $Ca2^+$ bound Gla domain of factor IX complexed with binding protein. J Biol Chem 278:24090–24094

Soriano-Garcia M, Padmanabhan K, de Vos AM, Tulinsky A (1992) The $Ca2^+$ ion and membrane binding structure of the Gla domain of Ca-prothrombin gragment 1. Biochemistry 31:680–685

Zhang L, Castellino FJ (1993) The contribution of individual gamma-carboxyglutamic acid residues in the calcium dependent binding of recombinant human protein C to acidic phospholipd vesicles. J Biol Chem 268:12040–12045

Zhang L, Castellino FJ (1994) The binding energy of human coagulation protein C to acidic phospholipids vesicles contains a major contribution from leucine 5 in the γ-carboxyglutamic acid domain. J Biol Chem 269:3590–3595